Feasibility Study and System Design for a Spaceborne Along-track Interferometer/Scatterometer

Delwyn Moller, Brian D. Pollard, and Ernesto Rodríguez
Jet Propulsion Laboratory
California Institute of Technology
4800 Oak Grove Drive
Pasadena, CA 91109
contact: delwyn.moller@jpl.nasa.gov

1 Introduction and Motivation

This paper presents a concept for measuring ocean surface current and unambiguous wind vectors using a spaceborne, squinted beam along-track interferometric (ATI) synthetic aperture radar (SAR). These kilometer-scale measurements would provide compelling data for coastal monitoring and characterization, enabling the observation of phenomena such as small-scale eddies, fresh-water discharge and atmospheric boundary layer turbulence signatures.

The complex dynamics of coastal zones, coupled with their ecological and anthropogenic importance, occur at spatial and temporal scales for which observations are extremely limited. In situ sensors (drifters) can be expensive, difficult to deploy and are limited in coverage. Shore-based high frequency (HF) radars are well proven at capturing surface current variability on resolutions of approximately 1 km, but these systems have limited global coverage.

Airborne ATI-SAR systems have demonstrated success in providing high-resolution images of surface currents [1], representative of spatially varying components of non-geostrophic circulation. Furthermore, there has been a great deal of interest and progress in utilizing SAR data for ocean-wind measurements at higher resolution than that possible from conventional scatterometer data [2, 3, 4]. The system proposed here may provide for significant improvements in SAR-based scatterometry by measuring back-scatter from distinct azimuthal directions, and by providing co-located surface currents.

2 Mission Design

Our design goal is to provide a system capable of high-resolution vector surface currents and wind-fields in the coastal regime while minimizing, to the full extent possible, the expected cost. As such, we have limited our considerations to a single spacecraft, and minimized mass, power, and data rate accordingly.

The high-level measurement requirements, listed in Tables 1 and 2, are similar in scope from those under development for NPOESS [5]. In this paper, we focus mainly on the surface current requirements (Table 1), although mention is made of future efforts toward satisfying Table 2.

The refresh rate is not mentioned in Tables 1 and 2. We have assumed a repeat cycle of 3-6 days at 800km, although this may not be sufficient for all coastal uses. Holt and Hilland [6] discuss some of the pertinent orbit issues and criteria.

Table 1: High level measurement requirements for coastal surface currents.

	System Capabilities	Requirement	Goal
1	Resolution	1.3 km	0.25 km
2	Measurement Range - speed	$0-5\ ms^{-1}$	$0-5\ ms^{-1}$
	Measurement Range - angle	$0-360^o$	$0-360^0$
3	Measurement Precision - speed	0.25 ms^{-1}	0.1 ms^{-1}
	Measurement Precision - angle	15°	5°
4	Measurement Accuracy - speed	0.25 ms^{-1}	0.1 ms^{-1}
	Measurement Accuracy - angle	15°	5°
5	Coastal Coverage	50 km	80 km

Table 2: High level measurement requirements for coastal winds. The footnoted items, speed precision and accuracy, denote a requirement with a percentage limit: i.e. the requirement may be stated as "2 ms^{-1} or 10%".

	System Capabilities	Requirement	Goal
1	Resolution	1.0 km	0.30 km
2	Measurement Range - speed	$3-35\ ms^{-1}$	$2-50\ ms^{-1}$
	Measurement Range - angle	$0-360^o$	$0-360^0$
3	Measurement Precision - speed[1]	2 ms^{-1}	1 ms^{-1}
	Measurement Precision - angle	15°	10°
4	Measurement Accuracy - speed[1]	2 ms^{-1}	1 ms^{-1}
	Measurement Accuracy - angle	15°	5°
5	Coastal Coverage	50 km	80 km

2.1 System Concept

Figure 1 shows the antenna illuminations assumed in this initial design. The configuration looks both fore and aft of the spacecraft for a total of four-beams, composed as two sets of two separated in the along-track dimension by a physical baseline B. The ability to reposition through scanning the elevation boresight allows the radar to optimize coastal coverage by following the coastline. The current design can scan an $80km$ swath between incidence angles $20° \leq \theta_i \leq 39°$, for a total viewing range of $\approx 300km$.

The squinted viewing geometries in Fig. 1 enable surface velocity vectors to be constructed from the ATI line-of-sight measurements. With both forward and aft squints, we are assured that at least one squint direction will not be cross-wind, where the ratio of approaching to receding Bragg-waves is unknown.

3 Nominal System Parameters

We have examined several choices of the system center frequency, including C-, Ku- and Ka-band. (Frequencies lower than C-band are not easily viable for a single spacecraft, while those above Ka-band may experience severe cloud and precipitation attenuation.) Ku-band, and to some extent C-band, are attractive due to the wealth of scatterometry experience. Additional key determining factors include the desire to minimize the physical along track baseline and total antenna size, the availability and maturity of technology, and oceanographic backscatter relevance and properties.

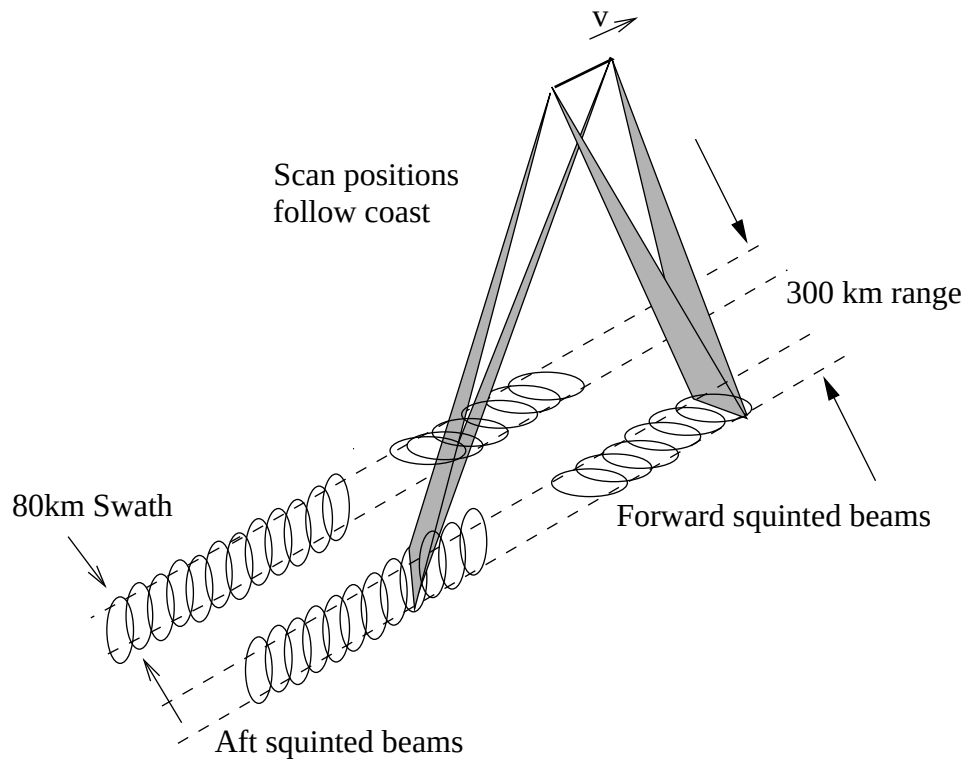

Figure 1: SAR configuration. Elevation scanning allow the system to track the coast line.

Balancing the above factors, we have chosen a Ku-band system.

The baseline and focused aperture lengths both depend on the ocean correlation time, τ_c. Following [7], we assume a Pierson-Mosokowitz-type spectrum, and estimate τ_c versus frequency as

$$\tau_c \approx 3\frac{\lambda}{u}\mathrm{erf}^{-1/2}(2.7\frac{\rho}{u^2}) \tag{1}$$

where ρ is the spatial resolution, λ is the electromagnetic wavelength, and u is the wind speed. Wind-speeds ranging from $u = 1\ ms^{-1}$ to $u = 10\ ms^{-1}$ result in correlation times between 7 and 70 ms, respectively, at Ku-band.

Table 3 shows the nominal system design parameters. The antenna size selected is $5 \times 0.25m$ as determined by azimuth ambiguities and the desired swath width. To obtain acceptable azimuth ambiguities while maintaining a reasonable antenna length, we selected a high prf with respect to the processing bandwidth. (The processing bandwidth lower limit is $B_p > f_d$ where f_d is the maximum Doppler-bandwidth over which the scene remains correlated.) Assuming long correlation times (ie low wind-speed) $f_d \approx 70Hz$.

The chosen bandwidth is 20MHz, resulting in an average operational data rate of $150Mb/s$. However, because this system is intended for coastal monitoring, the duty-cycle for data collection could be quite low, substantially reducing the average data rate.

4 System Performance

Table 4 summarizes the single-look system performance for the most distant (worst-case) sub-swath position. Over this sub-swath signal-to-noise ratio (SNR) is negative, although as we show in this section, this is not a real concern for the interferometric measurement.

Miller and Rochwarger [8] provide an asymptotic formula relating uncertainty in differential phase measurements to the SNR and the correlation coefficient, $\rho(\tau)$. Expressed in terms of Doppler

Table 3: Table of system parameters. See the text for detailed descriptions of each parameter.

Parameter	Value	Parameter	Value
Altitude	800 km	Orbital Velocity	7.47 km/s
Frequency	13400 MHz	Wavelength	2.237 cm
Elevation Boresight	31.96 deg	Azimuth Boresight	0 deg
Bandwidth	20 MHz	Noise Temperature	800 K
Clock Rate	45 MHz	Range Oversampling Factor	1.125
PRF	2246 Hz	Pulses in Air	15
Proc. Doppler Bandwidth	500 Hz	Azimuth Resolution	13.27 m
Swath Width	80 km	Beam-Limited Swath	95.88 km
Available Data Window	395.3 μs	IPP	445.3 μs
Transmit Peak Power	0.2 kW	Pulse Duration	50 μs
Radiated Power	22.46 W	System Losses	-4.5 dB
Non-TR DC Power	100 W	TR Module Efficiency	35%
DC Power	164.2 W	Duty Cycle	11.23%

velocity uncertainty, σ_v, it is

$$\sigma_v = \frac{\lambda}{2}\frac{\sqrt{(1+SNR^{-1})-\rho^2(\tau)}}{\sqrt{2N}2\pi\tau\rho(\tau)}, \tag{2}$$

where we have assumed a correlation function $\rho(\tau) = \exp(-(\frac{\tau}{\tau_c})^2)$, $N = N_{az}N_r$ is the number of independent looks, and τ is the image separation time $(= B/v)$.

The number of looks in range N_r is determined by the range pixel size divided by the number of range cells within that range pixel. The bandwidth results in a ground resolution O(10m) and yields N_r on the order of $23/pixel$ for the 250m pixel goal.

Because individual patches of surface are illuminated by the antenna for much longer than the coherence time, further independent looks at the surface are available. An approximate value for the number of available looks is given by the ratio of the time a given resolution cell is illuminated by the antenna to the coherence time, $N_{az} = T_{ill}/\tau_c$. Substituting for T_{ill}, we obtain:

$$N_{az} = \frac{R\lambda}{Dv_p\cos\theta_s\tau_c} \tag{3}$$

where R is slant range, D is the antenna physical aperture, v_p is the platform velocity, and θ_s is the squint angle, which we will neglect for now. Assuming $\tau_c = 10ms$, $N_{az} \approx 56$. The result is such that we can take advantage of $N = N_{az}N_r \approx 1288$ to substantially lower the velocity error in spite of the negative single-look SNR.

4.1 Baseline Length and System Precision

For a cost-effective spaceborne system meeting requirements with a reasonable interferometric baseline length $B = v_{sp}\tau$ is critical. The measurement range requirement dictates the upper bound for the baseline as follows:

$$-\frac{\lambda}{2\tau} < v_D < \frac{\lambda}{2\tau}. \tag{4}$$

The requirement is a measurement range of $0 - 5ms^{-1}$ or equivalently $\pm 2.5ms^{-1}$. To satisfy this $\tau \leq 2.2ms$ or $B \leq 15.4m$

The lower bound of the baseline is dictated by the desire for the baseline to be as short as possible while meeting precision requirements. Figure 2 illustrates the projected horizontal velocity

Table 4: Swath parameters for a single scan SAR position.

Data Swath	Start	Mid	End
Look Angle	30 deg	31.95 deg	33.81 deg
Incidence Angle	34.24 deg	36.56 deg	38.77 deg
Distance from Nadir	472.4 km	512.4 km	552.4 km
Slant Range	944 km	967.1 km	991.6 km
Time of Flight	6.297 ms	6.452 ms	6.615 ms
Range Resolution (ground)	11.53 m	10.9 m	10.36 m
Model σ^0	-11.65 dB	-13.2 dB	-14.66 dB
Total SNR	-2.574 dB	-0.4834 dB	-6.173 dB
$\mathrm{SNR_{max}}$	8.329 dB	10.64 dB	5.598 dB
Noise-Equiv. σ^0	-8.758 dB	-12.67 dB	-7.39 dB
Signal Level	-135.3 dB	-133.2 dB	-139 dB
Thermal Noise Level	-133.1 dB	-133.1 dB	-133.1 dB
ISLR	-15 dB	-15 dB	-15 dB
Quantization	-14.46 dB	-15.69 dB	-11.84 dB
Range Ambig	-12.73 dB	-26.91 dB	-8.173 dB
Az Ambig	-15.83 dB	-15.83 dB	-15.83 dB

precision as a function of baseline length evaluated at several (single-look) SNR's. We assumed that $\tau_c = 10ms$ and a ground resolution of $11m$.

The impact of the increasing wind speed on the correlation length (although not the backscatter) is shown in Figure 3. The higher wind speeds have no real impact until the baseline approaches $30m$.

4.2 Performance Impact Due to Squinting

While Madsen [9] and Frasier and Camps [7] have addressed the optimum fore/aft squint angle that minimizes the variance of the reconstructed velocity vector, neither considered the spaceborne case, where the look angles are typically much smaller, and the Earth's curvature becomes a significant factor. The optimization of the range loss, declining backscatter with increasing incidence, directional separation and surface projection effects leads one to look angles in the range of $20 - 30^o$, as we have chosen here. The ideal squint angle, when ground projected, is then also in the range of $20 - 30^o$, although it is of course a function of the swath position.

Two other factors also drive the choice of squint angle, and both also suggest that a more narrow angle is superior. Those factors are polarization losses and Doppler effects.

4.2.1 Polarization

As discussed in [10, 7], depending upon the choice of antenna architecture, the fore and aft squint of the sensor will have different polarization characteristics. One approach is to consider a nominally "side-looking" antenna that radiates fore- and aft-squinted beams (either simultaneous or switched). Another approach is to consider two physically different antennas oriented along the desired squint directions.

While the first approach is attractive, the combination of incidence angle and squint angle yields a polarization mixing such that the incident field on the ocean surface will consist of a combination of V and H polarizations (assuming a V-polarized transmitting antenna). This polarization mixing effect may be undesirable because the scattering amplitude is best understood (i.e. model functions exist) for V (or H) polarization at Ku-band. Modeling efforts may be complicated if two polarizations

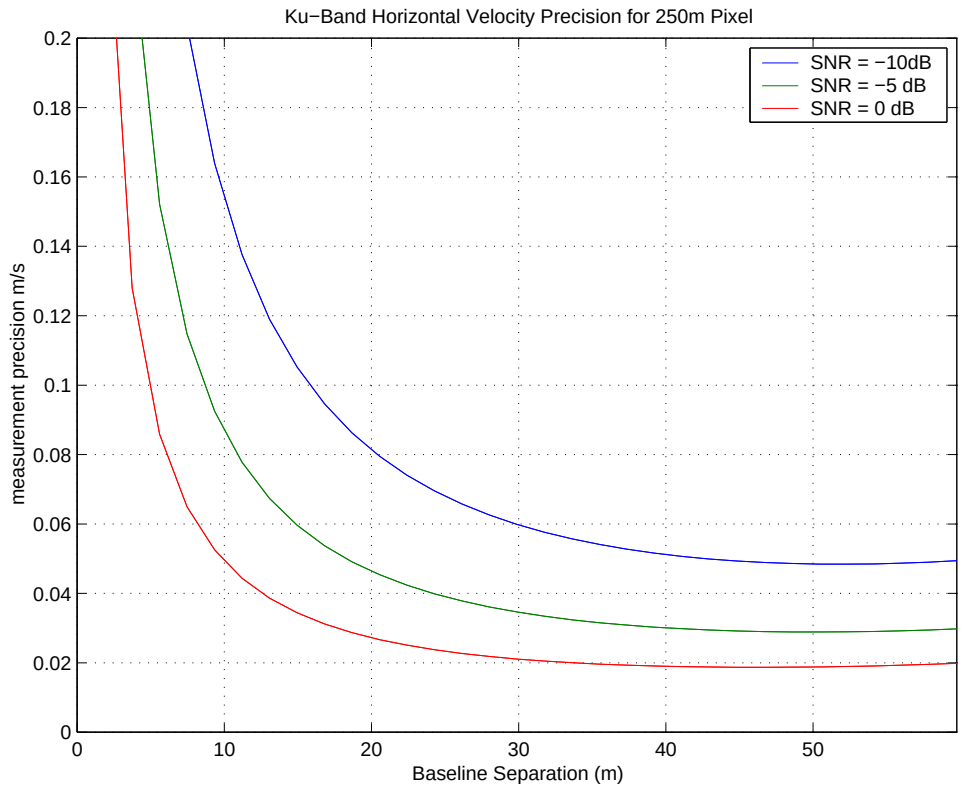

Figure 2: Tradeoff between SNR and decorrelation effects for interferometric measurement. Precision values are for ground projected velocity components.

must be considered. Furthermore, there will be some power-loss associated with the mixing effect. Minimizing the squint angles helps to mitigate this effect.

4.2.2 Doppler Effect

The large forward and aft squint angles proposed for this sensor impart large Doppler shifts on echo signals due to the component of the satellite's velocity vector in the direction of the radar beam. Moller et al. [10] showed that, in the case of a 45° squint, fore and aft squints can be separated by several hundred kilohertz. Further, the Doppler bandwidth is reduced as the squint angle increases, reducing the possible azimuth resolution and the available number of looks.

4.3 Requirement Compliance and Technology Feasibility

Based on the above discussion, the results in Figures 2 and 3, and a chosen squint angle of 22.5^o (see below), the required baseline length for requirement compliance can be derived. With an SNR in the range of -10dB, a baseline length of approximately $8m$ is sufficient to meet the requirements in Table 1.

The $8m$ baseline and the $5m \times 0.25m$ are the only significant technology challenges of the total system design (although they are quite similar to those being developed for the Wide Swath Ocean Altimeter [11]). The average and peak radiated power, system total power consumption, and system bandwidth are all quite modest when compared to modern SAR systems.

A number of designs for the antenna are available, as discussed in [9, 10, 7]. An actively steered antenna can certainly accomplish the $\pm 22.5^o$ chosen, although it could be considered the most massive and expensive option. A second possibility is to switch the phase of every other pair of antenna patches in azimuth, producing simultaneous beams at $\pm 22.5^o$, similar to the design first

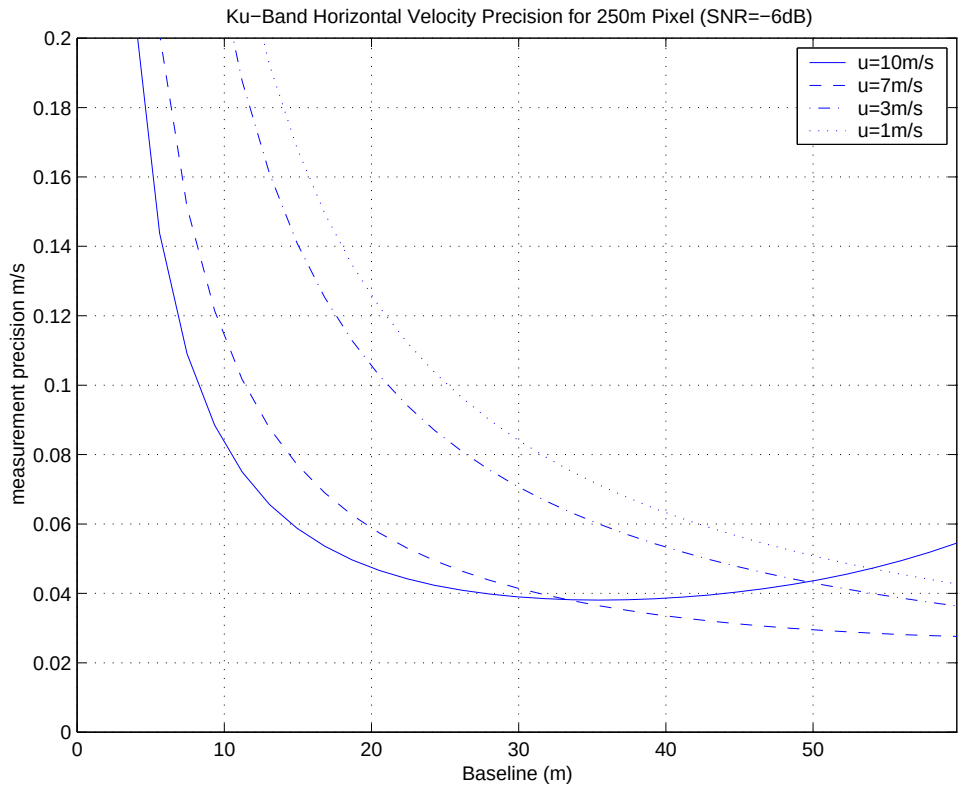

Figure 3: Effect of wind-speed on interferometric precision. As for Figure 2, precision values are for ground projected velocity components.

proposed by [9]. This design would still require a large (O(100)) number of transmit/receive (T/R) modules, however, and could weigh O($60kg$). Other, more advanced options could include active reflectarrays, or other multiple beam reflectors.

5 Surface Velocity Measurements, Construction of a Surface Current Vector and Unambiguous Wind Directions?

While the previous sections are concerned with the measurement velocity precision, the extraction of the current velocity from that measurement is not necessarily straightforward.

Radial surface Doppler velocity measurements, v_d can be expressed as

$$v_d = u_c + v_B + u_w \tag{5}$$

where u_c is the surface current, v_B is the phase velocity on the Bragg-resonant waves and u_w is the surface wind-drag. This equation assumes that v_d is measurement is over an extent large enough that the orbital velocities of the long waves average to zero. In reality, due to MTF effects there is usually a residual bias which will be discussed subsequently.

5.1 Bragg-wave Directional Spreading

One difficulty in estimating surface currents is uncertainty in the net component of velocity due to Bragg resonant waves. In particular, for viewing orientations off the wind axis, the relative contributions of both advancing and receding Bragg-waves is not well known. Thompson and Jensen [12] illustrated that this uncertainty can be a significant source of error. Toward this end Moller et

al. [13] found that their X-Band near-grazing observations followed a $cos^{2n}(\theta/2)$ analytical model for the directional spreading of the Bragg-waves. Of particular note is that the directional spreading was extremely broad for the 1.5cm Bragg waves observed. The implication is that, even significantly off the wind axis, the contribution of the Bragg velocity is the same as would be facing directly toward or away from the wind. Intuitively and theoretically this effect is prevalent at smaller Bragg-resonant wavelengths where the sensitivity to the wind is high. This concept is confirmed in the theoretical findings and simulations of Thompson and Romeiser [14].

The implication of this is that to correct for ATI measurements for the Bragg contribution, simply subtracting the Bragg-velocity consistent with the general viewing direction may be a fair assumption. To gauge this requires modeling and validation by ground-truthed data such as that collected in the current AirSAR campaign [15, 16].

5.2 MTF Effects

The effect of the Modulation Transfer Function (MTF) is to bias mean Doppler measurements because of the dependence of the backscattered power with the phase on the surface wave profile. Simply put, some parts of the wave produce more backscatter than others, so the mean reported Doppler shift is biased towards these portions of the wave. A substantial body of literature exists on field measurements of the MTF though little of the published literature directly addresses the impact of MTF on mean Doppler [13, 17]

6 Discussion

We find that a system design that meets the surface current precision requirements is quite feasible, and well within the bounds of modern technology. Open and substantial issues with the interferometric measurement include the measurement interpretation, discussed in the previous section, and the overall measurement accuracy, discussed in a companion paper by E. Rodríguez.

Finally, while we have not yet addressed the wind measurement capabilities of such a modest system, the drive for look angles in the $20 - 30^o$ range for the interferometric measurements could become a hindrance. Obtaining a balance between the two measurement techniques is an topic of ongoing work.

Acknowledgments

This work was performed at the Jet Propulsion Laboratory under contract with the National Aeronautics and Space Administration (NASA). The authors wish to thank David Imel for his SAR system analysis tool support.

References

[1] R. M. Goldstein, T. P. Barnett, and H. A. Zebker, "Remote sensing of ocean currents", *Science*, vol. 246, pp. 1282–1285, 1989.

[2] C. C. Wackerman, C. L. Rufenack, R. A. Schuchman, J. A. Johannessen, and K. L. Davidson, "Wind vector retrieval using ERS-1 synthetic aperture radar imagery", *IEEE Transaction on Geoscience and Remote Sensing*, vol. 36, no. 6, pp. 1343–1352, 1996.

[3] P. W. Vachon and F. W. Dobson, "Validation of wind vector retrieval from ERS-1 SAR images over the ocean", *The Global Atmosphere and Ocean System*, vol. 5, pp. 177–187, 1996.

[4] S. Lehner, J. Horstmann, W. Koch, and W. Rosenthal, "Mesoscale wind measurements using recalibrated ERS SAR images", *Journal of Geophysical Research*, vol. 103, no. C4, pp. 7847–7856, 1998.

[5] W. Pichel, "Ocean observer user requirements document", *Technical Report*, 2001.

[6] B. Holt and J. Hilland, "Rapid-repeat sar imaging of the ocean surface: are daily observations possible?", *Johns Hopkins APL Technical Digest*, vol. 21, pp. 7–14, 2000.

[7] S.J. Frasier and A.J.Camps, "Dual-beam interferometety for ocean surface current vector mapping", *IEEE Transaction on Geoscience and Remote Sensing*, vol. 39, no. 2, pp. 401–414, 2001.

[8] K.S. Miller and M.M. Rochwarger, "A covariance approach to spectral moment estimation", *IEEE Transactions on Information Theory*, vol. 18, no. 5, pp. 588–596, 1972.

[9] S. Madsen, "A dual aspect angle along track interferometer", *JPL interoffice memorandum*, , no. 3348-90-100, 1990.

[10] D. Moller, C. Werner, and S.J. Frasier, "Feasibility study and system design for a spaceborne along-track interferometer/scatterometer", Trade study report to nasa earth science and technology office, Jet Propulsion Laboratory, California Institute of Technology, Pasadena, CA, 1998.

[11] E. Rodriguez, B.D. Pollard, and J.M. Martin, "Wide swath ocean altimetry using radar interferometry", *IEEE Transaction on Geoscience and Remote Sensing*, in press.

[12] D.R. Thompson and J.R. Jensen, "Synthetic aperture radar interferometry applied to ship-generated internal waves in the 1989 loch linnhe experiment", *Journal of Geophysical Research*, vol. 98, no. c6, pp. 10259–10269, 1993.

[13] D. Moller, S.J. Frasier, D.L. Porter, and R.E. McIntosh, "Radar-derived interferometric surface currents and their relationship to subsurface current structure", *Journal of Geophysical Research*, vol. 103, no. C6, pp. 12839–12852, 1998.

[14] R. Romeiser and D.R. Thompson, "Numerical study on the along-track interferometric radar imaging mechanism on oceanic surface currents", *IEEE Transaction on Geoscience and Remote Sensing*, vol. 18, pp. 446–458, 2000.

[15] P.M. DiGiacomo, B. Holt, and L. Washburn, "An examination of small-scale coastal eddies and pollution hazards off California using an integrated multi-sensor/in-situ approach", *Proceedings of the 2002 AirSAR Symposium*, 2002.

[16] L. Washburn, P.M. DiGiacomo, and B. Holt, "Interpreting SAR imagery from surface currents obtained from high frequency radar near Point Conception, California", *Proceedings of the 2002 AirSAR Symposium*, 2002.

[17] R.D. Chapman, B.L. Gotwols, and R.E. Sterner II, "On the statistics of the phase of microwave backscatter from the ocean surface", *Journal of Geophysical Research*, vol. C8, pp. 16923–16301, 1994.